Colloid Polym Sci 277:1041–1050 (1999)

ORIGINAL CONTRIBUTION

F. Sauzedde
A. Elaïssari
C. Pichot

Hydrophilic magnetic polymer latexes. 2. Encapsulation of adsorbed iron oxide nanoparticles

Received: 28 December 1999
Accepted in revised form: 15 June 1999

F. Sauzedde · A. Elaïssari · C. Pichot (✉)
Unité Mixte CNRS-bioMérieux,
UMR-103 ENS-Lyon, 46 allée d'Italie
F-69364 Lyon Cedex 07, France
e-mail: christian.pichot@ens-bma.cnrs.fr
Tel.: +33-4-72728513
Fax: +33-4-72728533

Abstract The encapsulation of seed polymer particles coated by anionic iron oxide nanoparticles has been investigated using *N*-isopropylacrylamide as a main monomer, *N*,*N*-methylene bisacrylamide as a crosslinking agent, itaconic acid as a functional monomer and potassium persulfate as an anionic initiator. The magnetic latexes obtained have been characterized with regard to particle size, iron oxide content and electrophoretic mobility. All these properties have been examined by varying several polymerization parameters: reaction medium, monomer(s) and crosslinking agent concentrations, nature of seed latexes and type of polymerization (batch versus shot process). The magnetic content in the polymer microspheres strongly depends on the polymerization procedure (i.e., encapsulation process) and varies between 6 and 23 wt%, and monodisperse magnetic polymer particles were obtained.

Key words Encapsulation · Magnetic polymer particles · Hydrophilic · Submicron size · Carboxylic

Introduction

For many years, various strategies have been conceived and performed with a view to producing magnetic polymer particles for application in the biomedical field. Solid-phase immunoassays require microspheres with a narrow size distribution that exhibit a hydrophilic, biocompatible and functionalized surface for the covalent immobilization of proteins (such as antibodies, enzymes, etc.). In order to obtain submicron, monodisperse, hydrophilic, magnetic polymer microspheres, a three-step strategy is proposed.

1. The synthesis of three different monodisperse cationic seed polymer particles, polystyrene (PS) [2, 3], core–shell poly(styrene/*N*-isopropylacrylamide) [P(S/NIPAM)], as described elsewhere [4, 5], and pure P(NIPAM) microgels [6].
2. The adsorption of anionic magnetic nanoparticles onto these cationic polymer microspheres as reported in Ref. [1].
3. Seed precipitation polymerization of NIPAM.

In order to avoid iron oxide release or desorption, the last step is intended to encapsulate coated iron oxide nanoparticles. For more information on the adsorption study, the reader should consult Ref. [1].

This paper aims to describe the encapsulation step of the magnetic nanoparticles adsorbed onto PS and P(S/NIPAM) core–shell particles. Preliminary studies were performed to optimize the reaction medium, the recipe, the polymerization process and to check the reproducibility of encapsulation experiments. Potassium persulfate (KPS) was used as an anionic initiator and *N*,*N*-methylene bisacrylamide (MBA) as a crosslinker. In addition, itaconic acid (IA) was selected to provide surface carboxylic groups on the particles. Colloidal properties of the composite microspheres such as particle diameter, size distribution and electrophoretic mobility were determined. Moreover, the iron oxide contents and the magnetic properties of the magnetic particles prepared were also measured.

Experimental

Materials

Unless stated otherwise, reagents and solvents were used as received. Water was Milli-Q grade (Millipore, France) and was boiled for 2 h under a nitrogen stream before use. Styrene (Janssen Chemica, France) was distilled under reduced pressure; NIPAM (Kodak) was recrystallized in a 3/2 hexane/toluene mixture. KPS (Prolabo) was used as the initiator. MBA and IA bathophenanthroline disulfonic acid disodium salt hydrate, $FeSO_4{\cdot}7H_2O$, (Aldrich) were used as received.

Encapsulation of adsorbed iron oxide nanoparticles onto latex seeds

Before encapsulation, the excess free iron oxide particles were removed after 15 min incubation time by magnetic separation for 5–10 min and the supernatant was replaced by boiled and deoxygenated water before starting the polymerization. Encapsulation of adsorbed iron oxide nanoparticles onto various latex seeds was carried out in a 50-ml round-bottomed four-necked flask equipped with a glass anchor-shaped stirrer, condenser and nitrogen inlet. The temperature of the polymerization medium was maintained at 70 °C.

In accordance with Ref. [1], encapsulations were performed on several seed polymer particles coated with magnetic nanoparticles: PS (PS14) and P(S/NIPAM) core–shell latexes exhibiting different colloidal characteristics. The particle diameters of the seed latexes were measured both by quasielastic light scattering (QELS) at 20 and 40 °C and by transmission electron microscopy (TEM). As reported in Table 1, the seed particles are monodisperse and the thermal sensitivity of the P(S/NIPAM) core–shell particles is evident through the hydrodynamic diameter decrease at 40 °C [4, 5].

Precipitation polymerization of a mixture of NIPAM, MBA, IA and KPS was carried out according to the following conditions. Monomers solubilized in water were introduced in one or more shots. The final reaction volume was between 35 and 45 ml, with an initial solid content between 1 and 1.3%. The weight percentage of NIPAM with respect to seed polymer particle weight varied from 25 to 40%. The molar percentage over NIPAM of KPS was kept constant at 2%, MBA and IA molar percentages were between 1.2 and 7.2% and 0 and 6.3%, respectively. The polymerization conversion was determined according to the weight of the corresponding water soluble polymers (WSP) formed.

A series of composite latexes was produced by batch polymerization using the P(S/NIPAM)3 sample as a seed by varying the MBA and IA concentrations according to the recipe described in Table 2. Another series was obtained by varying the polymerization process according to the recipe given in Table 3.

Physicochemical and colloidal properties of magnetic latexes

Magnetic properties of composite particles

Magnetic measurements were carried out on the Automatic Bench of Magnetic Measurements (ABMM), CNRS-IRC, Villeurbanne. The magnetization of the ferrofluids was investigated by decreasing the magnetic field from 20000 to −500 œrsteds. The diamagnetic value of water was subtracted in order to take into account only the magnetic properties of the ultrafine particles.

Determination of magnetic particle content

The iron oxide content in the final latexes was determined both by a physical and a chemical method.

1. The magnetization variation as a function of the applied magnetic field was recorded on the ABMM. The saturation magnetization (M_s) corresponds to the plateau value of magnetization at high magnetic field values and the magnetic particle content (W_{mag}) was calculated from the experimental standard curve of the amount of iron oxide versus M_s.
2. Chemical titration based on the complexation reaction of bathophenanthroline disulfonic acid disodium salt wit Fe^{2+} ion in acidic medium [7, 8] was used by establishing a calibration curve using a $FeSO_4$ solution. In the acidic medium, iron oxide particles contained inside polymer particles were degraded and transformed into Fe^{2+} ions. The formation of the read complex was monitored from the optical density change at 535 nm using a Uvikon 930 spectrophotometer.

Particle size and distribution

The particle size and distribution of the magnetic latexes were determined by TEM and QELS. The particle morphology of the final magnetic polymer latexes was examined by scanning electron microscopy using a Hitachi S800, CMEABG, at the C. Bernard University, Lyon I, France.

Electrophoretic mobility measurements

Experiments were carried out with a Zeta Sizer III (Malvern Instruments England) at 20 and 40 °C. Latex electrophoretic mobilities were obtained in 10^{-3} M NaCl solution and as a function of pH.

Table 2 Encapsulation recipes as a function of *N*,*N*-methylene bisacrylamide (*MBA*) and itaconic acid (*IA*) proportions [mol %/*N*-isopropylacrylamide (*NIPAM*)]. W_{NIPAM} = 25 wt%/seed particles poly(styrene/NIPAM)3 [*P(S/NIPAM)3*], M_{KPS} = 2.1% (mol %/NIPAM), theoretical final solid content 1.70%

Code	M_{MBA}	M_{IA}
ML7	3.6	0
ML10	3.9	3.25
ML13	3.6	6.3
ML14	1.2	2.9
ML10	3.9	3.25
ML15	7.2	3.15

Table 1 Particle size characteristics of seed latexes as measured by quasielastic light scattering (D_h) at 20 and 40 °C, number average diameter ($\bar{D}_n$) and polydispersity index (*PDI*) as determined by transmission electron microscopy

Seed latex	$\bar{D}_n$ (nm)	PDI	D_h (20 °C) (nm)	D_h (40 °C) (nm)	Ref.
PS14	320	1.002	360	–	[2]
P(S/NIPAM)3	320	1.050	570	350	[3]
P(S/NIPAM)24	475	1.010	695	550	[1]
P(S/NIPAM)25	475	1.020	690	540	[1]
P(S/NIPAM)23	660	1.003	1050	860	–

Table 3 Encapsulation recipes according to various processes, (W_{NIPAM} wt%/seed particles) [P(S/NIPAM)23]; M_{MBA}, M_{KPS} and M_{IA} (mol %/NIPAM)

Code	Process	W_{NIPAM}	M_{MBA}	M_{KPS}	M_{IA}
ML16	Shot at 0 h	33 (St)[a]	11 (NIPAM)[b]	1	0
	Shot at 14 h	7.6	3	1.9	13
ML17	Batch	30	4.3	1.75	0
ML18	Batch	30	4.0	2.1	3.1
ML19	Shot at 0 h	35	4.7	1.9	0
	Shot at 20 min	35	1.8	0	2.4
ML20	Shot at 0 h	30	1.95	1.87	0
	Shot at 30 min	30	3.6	1.88	0
	Shot at 30 min	30	4.72	0	3.24

[a] Weight ratio the amount of styrene over seed polymer particle
[b] Weight ratio to the amount of NIPAM over styrene

Table 4 Encapsulations in various reaction media: iron oxide content (W_{mag}), number of magnetic separations before polymerization and pH of uncleaned latexes. Polymerization recipe W_{NIPAM} = 40 (wt%/seed particles [P(S/NIPAM)25], M_{MBA} = 4, M_{KPS} = 2, M_{IA} = 3 (mol%/NIPAM), theoretical final conversion was from 1.7 to 2%

Code	Reaction medium	W_{mag} (wt%)	Cleaning	pH
ML1[a]	Water	10	1	5.4
ML2	Iron oxide dispersion	5	0	8.6
ML3	Water	11	3	3.5
ML4	Citrate 5×10^{-3} mol/l	6	1	6.5
ML5	NaOH 10^{-3} M	13	1	7.3

[a] Latex seed was P(S/NIPAM)24

Results

Due to the electrostatic nature of the interactions between magnetic-nanoparticle-coated seed particles and polymer chains growing during the encapsulation step, the influence of pertinent variables such as pH, the nature of the reaction medium and the amount of the main monomer was investigated first.

Preliminary study

Influence of reaction medium on the encapsulation step

Encapsulations were performed under different polymerization conditions such as pH, ionic strength and also the presence or the absence of free iron oxide nanoparticles in the polymerization medium as described in Table 4. As expected, the numbers of encapsulated nanoparticles are drastically affected by the reaction medium. In fact, comparison of magnetite contents (W_{mag}) between ML1 and ML2 experiments seems to indicate that the presence of ferrofluid is unfavourable for an efficient encapsulation process. This behaviour can be attributed to the role of free iron oxide nanoparticles leading to the inhibition of encapsulation magnetic-nanoparticle-coated seed polymer particles. The amount of encapsulated iron oxide is similar when polymerization is carried out in the presence either of the free nanoparticles (ML2) or of free citrate anions (ML4). By adding a citrate solution, the ionic strength is increased to 3.0×10^{-2} leading to a decrease in the amount of magnetic material incorporated. In this case, the affinity between new polymer chains and seed particles is enhanced compared to electrostatic interactions between magnetic nanoparticles and latex which might be decreased by charge-screening. Nevertheless, in the presence of a large number of magnetic nanoparticles in the reaction medium, no encapsulation was observed. Moreover, the polymerization pH does not seem to affect the number of nanoparticles incorporated (ML3, ML1 and ML5).

Effect of the amount of NIPAM monomer introduced

In order to enhance the thickness of the hydrophilic surface layer and to allow a better encapsulation of iron oxide particles, the weight percentage (referred to seed particle amount) of the main monomer (W_{NIPAM}) was increased from 25 to 42%, all other reactant concentrations being kept constant with respect to the NIPAM amount (Table 5). The final particle size was measured by both QELS and TEM. The hydrodynamic particle diameter drastically increases upon increasing the monomer concentration, reflecting the encapsulation of the adsorbed iron oxide nanoparticles onto seed microspheres. As can be seen in Table 5, the iron oxide content (≠13 wt%) is not affected by the amount of NIPAM added whereas the WSP proportion rises from 12 to 27%. The results from TEM reflect the fact that the final latexes exhibit a narrow size distribution; no secondary nucleation occurred. The large values of the hydrodynamic diameter can be mainly attributed to the presence of a small fraction of aggregated particles or to the bridging flocculation induced by the large degree of WSP formation, as for ML12. The electrophoretic mobility values measured at 20 °C and pH 10 (see Table 5) decrease with increasing amount of added monomers, indicating that either the electrostatic stabilization is reduced, due to a decrease in the amount of

Table 5 Influence of the amount of monomer added: diameter ($\bar{D}_n, D_h$), water soluble polymer (*WSP*) amount, W_{mag}, electrophoretic mobility (μ) at pH 10 at 20 and 40 °C (in units of 10^{-8} m^2/Vs) and the isoelectric point (*PI*). Polymerization recipe: W_{NIPAM} in wt%/seed particle (PS14), M_{MBA} = 3.8, M_{KPS} = 2.1, M_{IA} = 3.0 (mol%/NIPAM), theoretical final solid content = 1.70%

Code	W_{NIPAM} (wt %)	$\bar{D}_n$	PDI	D_h	WSP (wt%)	W_{mag} (wt%)	μ (20 °C)	μ (40 °C)	PI
ML9	25	346	1.003	460	12	14	−2.5	−5.9	4
ML11	30	337	1.004	800	22	12.5	−1.5	−5.6	4
ML12	42	329	1.004	1040	27	13	−1.1	−5.2	< 3

Table 6 Reproducibility study: particle size, pH, μ at 20 and 40 °C (in units of 10^{-8} m^2/Vs) encapsulated nanoparticle amount (W_{mag}) and WSP amount. Polymerization recipe: W_{NIPAM} = 25 wt%/seed particles P(S/NIPAM)3, M_{MBA} = 3.6, M_{KPS} = 1.5, M_{IA} = 0 (mol%/NIPAM), theoretical final solid content = 1.70 (wt%)

Code	$\bar{D}_n$	PDI	D_h	pH	μ (20 °C)	μ (40 °C)	W_{mag} (wt%)	WSP (wt%)
ML6	380	1.02	670	–	–	–	27	9.4
ML7	341	1.01	650	7.15	−2.5	−4.5	26	8.7
ML8	352	1.03	860	7.35	−2.5	−4.5	26	5

Table 7 Influence of the nature of seed particles on the weight percentage of magnetic nanoparticles before (W_{ads}) and after (W_{mag}) encapsulation. μ (in units of 10^{-8} m^2/Vs) at 20 and 40 °C at 10^{-3} ionic strength and pH 10, weight percentage of WSP. Polymerization recipe: W_{NIPAM} = 25 wt%/seed latex, M_{MBA} = 3.85, M_{KPS} = 2.1, M_{IA} = 3.2, (mol%/NIPAM), theoretical final solid content = 1.70%

Code	Seed latex	Adsorbed (W_{ads}, wt%)	Encapsulated (W_{mag}, wt%)	μ (20 °C)	μ (40 °C)	WSP (wt%)
ML9	PS14	29	14.5	−2.5	−5.9	12
ML10	P(S/NIPAM)3	48	23	−1.35	−4.8	17

functional monomer (IA) incorporated, or that the presence of a thicker layer influences more significantly the slipping plane and, as a consequence, the electrophoretic values.

Reproducibility study

Finally, the encapsulation reproducibility was also checked by performing three encapsulations under identical conditions, using the seed particles and recipe described in Table 6. No significant difference was observed when considering particle diameter, size distribution, electrophoretic mobility and iron oxide content. Nevertheless, there could be some variation in the hydrodynamic diameter of the composite microspheres due to the presence of aggregated particles. In addition, the magnetic latexes prepared exhibit the same properties such as electrophoretic mobility (at 20 and 40 °C), magnetic content ($W_{mag} \sim 26$ wt%) and have similar WSP amounts.

Based on this preliminary study, further encapsulation experiments were conducted by directly replacing the excess nanoparticles by degassed and boiled water and the amount of added NIPAM was limited to 25% with respect to seed polymer particle weight.

Influence of the type of seed particles

As previously shown [1], the nature of the seed microspheres was found to drastically affect the amount of iron oxide adsorbed. In fact, the number of nanoparticles adsorbed was found to be higher in the case of core–shell and pure P(NIPAM) microspheres than in the case of PS particles (Table 7). Thus, it is expected that the number of iron oxide nanoparticles encapsulated should likewise depend on the type of seed particles.

From TEM micrographs of encapsulated ML9 and ML10 latexes (Fig. 2), no second population of polymer particles appears and the weight percentage values of WSP chains are near 15%. These two features confirm that encapsulation mainly took place within and onto a coated seed polymer surface.

Based on the results reported in Ref. [1], some encapsulations were also carried out using pure P(NIPAM) microgel particles as seeds in order to further increase the final magnetic material content. Precipitation polymerization of NIPAM was first performed in conditions similar to that of experiments ML9. From TEM micrographs (Fig. 3) it seems that iron oxide particles are distributed around a polymer core, which suggests that release took place during the encapsulation. So far, we have no clear explanation to

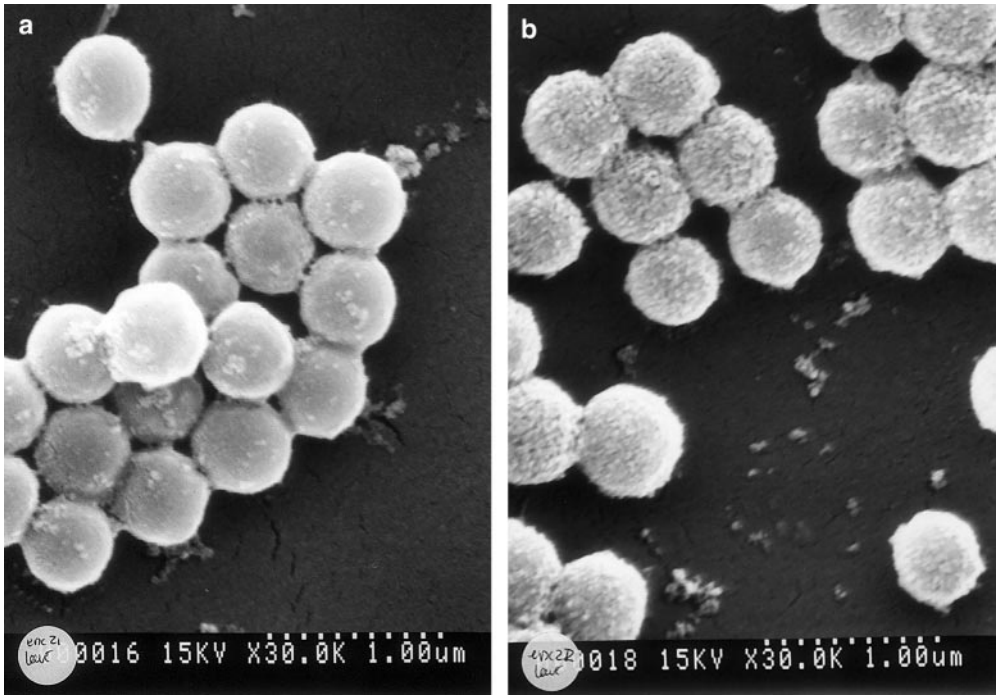

Fig. 1 SEM micrographs. **a** Scanning electron microscopy (SEM) image (×30000), run ML2, low magnetic nanoparticle content. **b** SEM image (×30 000), run ML3, high magnetic nanoparticle content

interpret this result and more experiments are underway to gain more insight. No more experiments were carried out using P(NIPAM) particles.

Magnetic material content

As already reported [1], a high amount of adsorbed iron oxide was obtained in the case of the core–shell latex (48 wt%) compared to the smooth PS latex (29 wt%) and a high number of encapsulated nanoparticles onto the core–shell latex is observed, as expected (Table 7).

In the case of core–shell particles, it seems that some of the adsorbed nanoparticles are not strongly incorporated within the P(NIPAM) layer. As shown in Ref. [1], P(NIPAM) chains are swollen by water and allow iron oxide particle diffusion into the hairy layer. Some of the magnetic nanoparticles are attracted by electrostatic interactions, and some are only physically entrapped in the hairy layer; this can easily be desorbed during polymerization, storage or washing leading to a lower encapsulated amount (23%) compared to that of the initial amount of iron oxide adsorbed (48%). In contrast, in the case of PS particles, neither water nor ferrofluid penetrate into the polymer particles and interactions between inorganic and polymer particles occur more strongly at the water–polymer interface. Even if the amount adsorbed is lower, electrostatic interactions should be strong enough to reduce the desorption phenomenon. Moreover, as far as thermodynamics is concerned, adsorption is more favoured onto a smooth PS particle surface than onto a hairy P(NIPAM) hydrogel. Indeed, it may be considered that adsorption of magnetic nanoparticles is more entropically favourable onto plain cationic hydrophobic microspheres than onto the hairy layer of core–shell particles.

Electrophoretic mobility

With both types of seed particles, the electrophoretic mobility values of the final magnetic particles are larger at 40 °C than at 20 °C. As already reported by Fujimoto et al. [9], this behaviour reflects the thermal sensitivity of the magnetic latexes, which is attributed to the presence of P(NIPAM). In fact, in the case of run ML9 (using PS seed particles), the electrophoretic mobility increased on raising the temperature above 32 °C, which is indicative that the final composite particles also exhibit a P(NIPAM) hydrophilic layer.

Effect of polymerization recipe

The influences of the crosslinker agent (MBA) and the functional monomer (IA) concentrations on the encapsulation of adsorbed iron oxide nanoparticles onto core–shell latex P(S/NIPAM)3 were studied according to the recipes reported in Table 2. The properties of the final latexes are reported in Table 8.

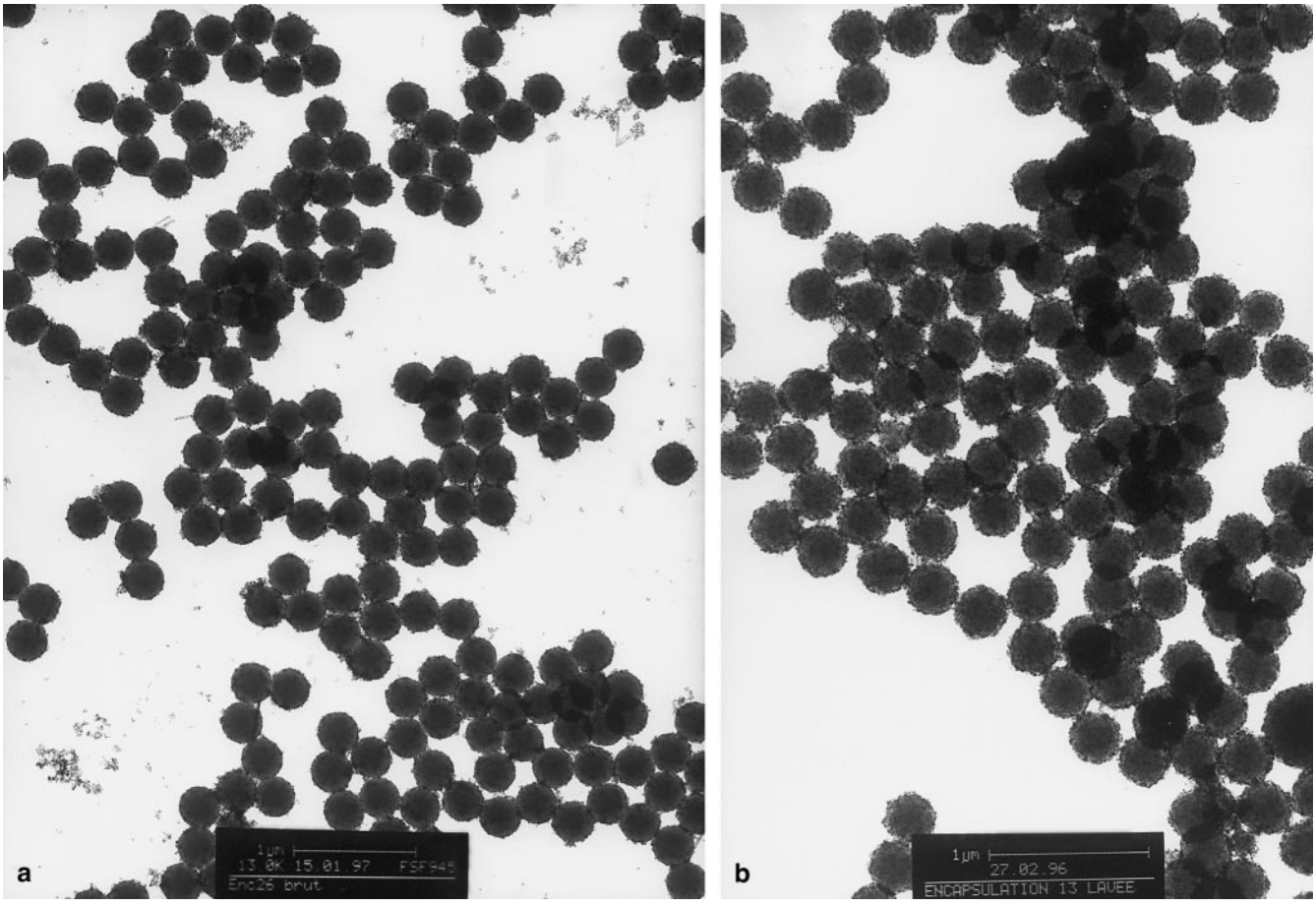

Fig. 2 TEM micrographs. **a** Transmission electron microscopy (TEM) image, run ML11, monodispersed uncleaned latex using PS14 as seed particles. **b** TEM image, run ML8, monodispersed uncleaned latex using poly(styrene/*N*-isopropylacrylamide)3 [P(S/NIPAM)3] as seed particles

Iron oxide content

The numbers of adsorbed iron oxide nanoparticles encapsulated onto core–shell microspheres were determined by varying the proportion of MBA and IA in the polymerization recipe. In fact, upon raising both functional monomer (IA) and crosslinker (MBA) concentrations, the number of magnetic nanoparticles incorporated by encapsulation slightly decreases from 26% to 14%, and from 21% to 17%, respectively. A reduction in the iron oxide content during encapsulation can occur for two reasons.

1. Desorption of adsorbed iron oxide induced by negatively charged WSP which may act as competing agents in the adsorption process as stabilizers of desorbed nanoparticles.
2. Shrinkage of the P(NIPAM) shell ''bearing iron oxide nanoparticles'' induced by polymerization temperature (70 °C) can lead to an increase in the nanoparticle desorption as evidenced in Ref. [1].

Excessively high concentrations of IA and MBA result in a decrease in the amount of encapsulated iron oxide and also favour undesirable WSP formation. Nevertheless, MBA and IA monomers should be introduced in appropriate concentrations, i.e., 3 and 4 mol% relative to NIPAM, respectively, to ensure both P(NIPAM) chain incorporation (MBA) and significant surface carboxylic charge on the particles (IA).

Colloidal properties

The particle sizes measured by QELS are larger than expected; this can be due to the presence of few aggregated particles and also to the complexity of the particle structure. This can be attributed to the aggregate formation during the encapsulation step since the pH of the medium is controlled by both iron oxide dispersion (pH close to 8) and IA concentration. At high IA concentration, the pH decreases as shown in Table 8. The carboxylic groups are only partially dissociated, thereby reducing electrostatic stability during polymerization. Furthermore, due to the water solubility of IA,

the amount of WSP increases greatly upon increasing its concentration, which could affect the colloidal stability as discussed previously. Anyway, the particle size and size distribution as deduced from TEM reflect the presence of a second population of particles for high MBA concentrations such as 7.2 wt% (run ML15), whereas no secondary nucleation is observed in the functional monomer concentration range investigated and for low MBA concentrations as reported in Table 8.

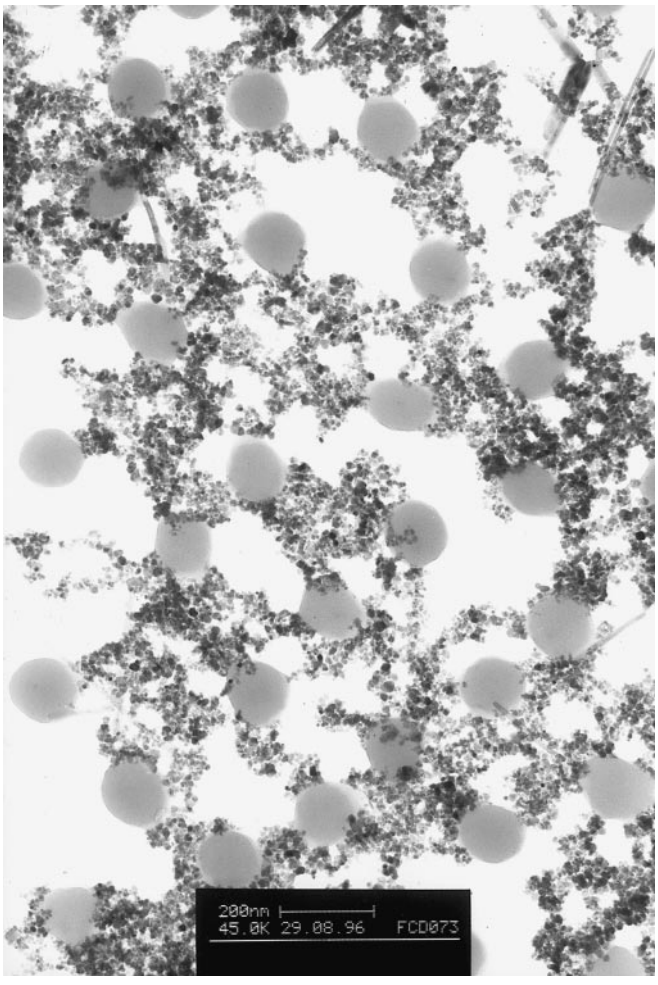

Fig. 3 TEM image, uncleaned latex using whole P(NIPAM) microspheres are seed particles

According to the interface complexity of the magnetic latex particles prepared, only two points can be deduced from the electrophoretic mobility measurements.

1. All latexes produced are negatively charged and are thermosensitive since the electrophoretic mobility increases with increasing temperature.
2. The isoelectric point (PI) was found to be close to the pK_a of the carboxylic groups, reflecting the possible incorporation of functional monomer (IA).

Effect of polymerization process (batch versus shot)

More experiments were carried out to improve the encapsulation performance by sequentially addition of MBA and IA during the encapsulation step.

The shot encapsulation process consists of adding the whole monomer mixture in several steps (or additions), the first shot charge containing all monomers with a low proportion of IA, whereas in the last stage the remainder of IA is introduced. With large seed P(S/NIPAM) core–shell particles, encapsulations were performed either using a batch process (runs ML17 and ML18 without and with IA, respectively), or different shot additions as described in Table 3. With a shot process, carboxylic monomer (IA) was introduced in the last step so as to reduce WSP formation and to favour the incorporation of carboxylic groups onto the particle surface. The crosslinker concentration was either increased at each step of the polymerization (run ML20), or decreased (run ML19). The reason for adding styrene instead of NIPAM in the first shot of the process (ML16) was to compare the influence of both types of polymer (hydrophilic versus hydrophobic) on the incorporation of magnetic nanoparticles. According to the characteristics of the final composite particles given in Table 9, some remarks may be raised concerning the iron oxide content and particle stability.

Iron oxide content

At first sight, the introduction of styrene in the initial step of shot addition (run ML16) did not affect the amount of iron oxide incorporated in comparison with the batch process using NIPAM (run ML17). In fact, the

Table 8 Influence of MBA and IA concentrations on properties of magnetic latexes: final particle diameter ($\bar{D}_n$) PDI, hydrodynamic diameter (D_h), encapsulated iron oxide amount (W_{mag}), at pH 10 at 20 and 40 °C (in units of 10^{-8} m^2/Vs), weight percentage of WSP and pH of uncleaned magnetic latexes

Code	$\bar{D}_n$ (nm)	PDI	D_h (nm)	W_{mag} (wt%)	μ (20 °C)	μ (40 °C)	PI	WSP (wt%)	pH
ML7	341	1.01	650	26	−2.27	−4.5	5	8.7	7.15
ML10	382	1.03	1200	23	−1.02	−4.24	4/4.5	17	6.25
ML13	331	1.01	900	14	−2.12	−5.80	4/4.5	19	5.60
ML14	335	1.01	1200	21	−2.20	−5.70	4	22	6.36
ML10	382	1.03	1200	23	−1.35	−4.80	4/4.5	17	6.25
ML15[a]	343	1.01	950	17	−1.35	−4.85	4/4.5	19	6.30

[a] Second nucleation

Table 9 Influence of the polymerization process on the colloidal properties of magnetic particles: $\bar{D}_n$, PDI, D_h, W_{mag}, at pH 10 at 20 and 40 °C (in units of 10^{-8} m^2/Vs), weight percentage of WSP and pH of uncleaned magnetic latexes

Code	$\bar{D}_n$ (nm)	PDI	D_h (nm)	W_{mag} (wt%)	μ (20 °C)	μ (40 °C)	PI	WSP (wt%)	pH
ML16	648	1.005	1000	12.5	–	–	–	12	6.60
ML17	716	1.002	1050	12.5	−1.45	−4.60	3.5	27	7.10
ML18[a]	619	1.003	1100	7	−1.24	−4.10	4/4.5	25	5.35
ML19[a]	721	1.003	1100	11	−0.91	−4.71	3.5	40	5.45
ML20[a]	704	1.006	1110	6.5	−0.43	−2.86	4	38	6.35

[a] Second nucleation

QELS particle size was found to be in the same range and the amount of iron oxide encapsulated was 12.5 wt% irrespective of the polymerization process. Nevertheless, in the former case, the measured particle size using QELS is higher than expected, a result which can be explained by the presence of unstable particles undergoing aggregation. By increasing the crosslinker agent (MBA) concentration at each step of the shot process (run ML20) or in the presence of IA (run ML18), the iron oxide content (W_{mag}) was lowered from 12 to 6.5 and 7 wt%, respectively. In contrast, in run ML19, where the total amount of MBA is low, W_{mag} is more important. This confirms the paramount influence of MBA concentration on the nanoparticle encapsulation.

Shot processes performed with NIPAM provided a large amount of WSP (40%, run ML19), instead of 12% when styrene was added in the first step in spite of the large amount of IA added in the second step of the addition process. In this case, new oligomer chains containing styrene units are more hydrophobic, which makes it easier for them to be captured by seed particles. Moreover, by adding IA in one or several stages, a secondary nucleation appears (ML19, ML20, ML18) which favours WSP formation. Such generation of new particles should depend on the relative concentration of monomer added with respect to the overall surface area provided by the seed particles [10]. In the case of encapsulations carried out with IA, the oligomer formation is greatly enhanced, explaining the high percentage of WSP. These IA-rich growing polymer chains with hydrophilic character cannot be captured easily by relatively hydrophobic seed particles and stay preferentially in the aqueous phase where they can lead to new particles through a homogeneous (or micellar) nucleation mechanism. This is well exemplified by comparing ML17 and ML20 experiments, where a second nucleation was observed when only IA was added (ML20). In contrast, with the hardly water soluble styrene, most of the monomer diffuses into the polymer particles, which disfavours a second nucleation stage [10].

Colloidal stability

The particle size does not appear to be process-dependent. The differences between TEM and QELS values are significant, revealing the hydrophilic P(NIPAM) layer at the surface of the encapsulated nanoparticles. No dramatic increase in particle size is evident from comparisons of QELS and TEM values. It can also be supposed that no particle aggregates are formed in these series of latexes. Large differences in electrophoretic mobility values (Table 9) are observed for the different encapsulations. Since electrophoretic mobility or isoelectric potential values are influenced by the interfacial P(NIAPM) layer thickness, the availability of carboxylic groups and the presence of nanoparticles, one cannot correctly correlate the electrokinetic behaviour to the surface carboxylic groups.

Discussion

According to various experimental observations and from studies reported by other authors, several points are worth discussing in relation to the polymerization mechanism leading to the production of these composite particles and their colloidal and magnetic properties.

Polymerization onto inorganic particle surfaces

Precipitation polymerization of NIPAM was generated using a negatively charged initiator to encapsulate particles bearing charges of the same nature. Such a strategy was also followed by Furusawa et al. [11] and Yanase et al. [12], who used KPS to initiate emulsion polymerization of styrene on iron oxide particles coated with an anionic surfactant; however this method was questioned by other authors [13, 14] who reported a large decrease in the polymer yield and the formation of a second population of polymer particles when the initiator and the inorganic particles bore charges of the same nature. In this case although electrostatic repulsions are strong, polymerization can occur at an inorganic particle surface through chemical affinity. In contrast, with an initiator oppositely charged to the seed particles, the new oligomers can be adsorbed (via attractive electrostatic interactions) onto seed microsphere surfaces, causing an increase in the polymer yield.

In our case, a second population of polymer particles was obtained in the presence of seed microspheres of

large size by introducing monomers in several shots or by adding relatively high concentrations of IA monomer. The formation of new tiny particles was attributed to a low surface-capture efficiency and the hydrophilicity of the oligomers. Moreover, seed particles constituted of a polymeric core coated by nanoparticles exhibit a heterogeneous surface structure. Encapsulation of these heterocoagulates cannot be straightforward compared to polymerization performed only in the presence of inorganic particles.

In the literature, the polymerization at an inorganic surface is reported to be feasible after particle surface modification [14]. This can be accomplished either by physical adsorption of a surfactant [7, 12] or a polymer [15] onto iron oxide nanoparticles, or by chemical grafting of a coupling agent [16, 17] onto silica or rutile nanoparticles. In our case, the affinity is provided by the presence of citrate molecules at the surface of the nanoparticles. Both electrophoretic mobility measurements and the low amount of WSP recovered suggest that polymerization occurred mostly on the seed particle surface.

Particle stability

Magnetic polymer particles were found to settle rapidly due to the presence of the iron oxide material (density of 5.25 g/cm^3 for Fe_3O_4). Such sedimentation can eventually cause aggregate formation during storage. Nevertheless, magnetic particles can be stabilized both by electrostatic and steric repulsions provided by sulfate and carboxylic groups from the initiator fragments (IA) and P(NIPAM) chains, respectively. For example, in the case of large seed particles, the small difference between D_n and D_h can be assigned only to P(NIPAM) shrinkage. The magnetic nanoparticle content is low and electrosteric stabilization is efficient enough to prevent magnetic particle aggregation. Furthermore, the formation of a large amount of WSP can induce particle-bridging at room temperature. In experiments ML7 and ML9 (Tables 5, 6), low hydrodynamic diameter values can indirectly reflect a low percentage of WSP.

Iron oxide content

It is worth comparing results from magnetic and chemical titration of iron oxide, as given in Table 10. Both methods, performed on seven different samples, are in good agreement, proving the reliability of the chemical titration used for further titration. Special attention was given to the possible desorption of nanoparticles upon storage. Numerous washing steps were required to make sure that no more desorption occurred. The amount of iron oxide released was evaluated by comparing the weight percentage of magnetic material on cleaned latex just after washing ($W_{mag\text{-}1}$) and after several weeks under gentle agitation ($W_{mag\text{-}2}$) (Table 11). $W_{mag\text{-}1}$ was determined when the last supernatant was not coloured; however, after a few days under gentle agitation, the supernatant was again coloured, indicating a slow iron oxide desorption process. After extensive washing for a few weeks, the supernatant was found to be unchanged after 1 week of agitation: the new iron oxide content was then calculated, i.e., $W_{mag\text{-}2}$.

The ratio $\Delta D/D_h$ (ratio of the difference between D_h measured at 20 and 40 °C and the value of the hydrodynamic diameter measured at 20 °C) represents the contribution of the hydrogel layer to the overall seed particle diameter. In the case of small-seed core–shell particles [P(S/NIPAM)3], $\Delta D/D_h$ is large which explains the high number of magnetic nanoparticles before [1] and after encapsulation ($W_{mag\text{-}1}$). According to Table 11,

Table 10 Encapsulated magnetic nanoparticles amount (weight percentage) determined by chemical titration and by magnetization measurements

Code	Chemical titration	Magnetization measurement
ML10	28	33
ML13	22.4	23.2
ML18	17.7	17.5
ML16	12.7	12.5
ML3	12	13.1
ML9	18.8	19.2
ML1	11.2	12

Table 11 Desorption study: seed latex and relative hydrophilic shell thickness ($\Delta D/D_h$), weight percentage of nanoparticles calculated on cleaned latex just after washing ($W_{mag\text{-}1}$) and after several weeks under gentle agitation ($W_{mag\text{-}2}$)

Code	Seed latex	$\Delta D/D_h$	$W_{mag\text{-}1}$ (wt%)	$W_{mag\text{-}2}$ (wt%)
ML10	P(S/NIPAM)3	38	29	23
ML15	P(S/NIPAM)3	38	23	17
ML13	P(S/NIPAM)3	38	28	14
ML1	P(S/NIPAM)24	26	16.5	10
ML17	P(S/NIPAM)23	19	17	12
ML19	P(S/NIPAM)23	19	16	11
ML12	PS14	0	18	13
ML11	PS14	0	16	12.5
ML9	PS14	0	19	14

nanoparticle desorption depends on the type of seed particle and whatever the significance of the hairy layer (from 0 to 25%), the iron oxide content after encapsulation, $W_{mag\text{-}1}$, is about 17–18%. For example, for experiments carried out with P(S/NIPAM)3 as seed particles, the final iron oxide content is about 15%, except in the case of run ML10, where $W_{mag\text{-}2}$ is 23% because the particles formed aggregates during the washing procedure and desorption was less significant.

In the other runs, the amount of magnetic material desorbed is near 5% and $W_{mag\text{-}2}$ remains at approximately 12%. The desorption process is very significant for high $\Delta D/D_h$ (Table 11) values. The final iron oxide content obtained with P(S/NIPAM) as seed particles is a little larger than that obtained with PS ones.

Magnetic properties of composites particles

The composite latexes were examined with regard to their magnetic nature in relation to the weight percentage of iron oxide. In Ref. [1], the iron oxide dispersion was reported to exhibit superparamagnetic properties. Magnetization measurements were performed to verify whether or not these nanoparticles kept this property when incorporated inside the final magnetic particles. Magnetization was recorded upon decreasing the magnetic field. Figure 4 shows high plateau values depending on the iron oxide content and a rapid decrease of magnetization to zero when the magnetic field tends to zero, which corroborates the fact that the incorporated nanoparticles are still superparamagnetic.

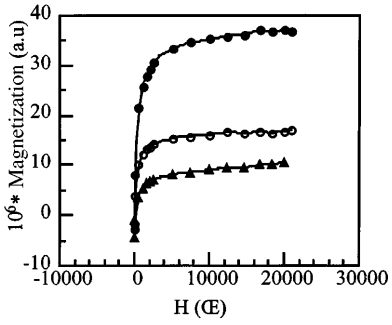

Fig. 4 Magnetization as a function of applied magnetic field for different ferrite contents. ML18(▲), ML13(○), ML3(●)

Conclusions

Superparamagnetic, hydrophilic, carboxylated and monodisperse microspheres were obtained by encapsulation of magnetic nanoparticle-coated polymer particles. Seed precipitation polymerization of NIPAM was carried out under various experimental conditions. No aggregation was observed and a second population of polymer particles was formed only in particular cases. Moreover, quite low amounts of WSP were left leading to the conclusion that P(NIPAM) is mainly formed and is anchored onto the particle surface.

Using a three-step procedure, the presence of the initial seed particles allows the final particle diameter range and the size distribution to be monitored. The amount of iron oxide incorporated largely depends on the polymerization recipe and only slightly on the nature of the polymer particles (hydrophobic versus hydrophilic). Nevertheless, one may expect larger amounts to be incorporated by using pure P(NIPAM) microgel particles or two hydrophilic polymers (one in the core, the other for the outer shell) exhibiting different lower critical solubility temperatures: these alternative routes should be investigated in more detail.

Due to their size and surface hydrophilicity, these well-characterized and monodisperse magnetic particles should be good candidates for solid phases in immunoassays. The presence of a P(NIPAM) shell should avoid nonspecific immobilization of proteins and the presence of carboxylic groups provided by the functional monomer would allow, after activation, covalent binding of proteins.

References

1. Sauzedde F, Elaïssari A, Pichot C (1999) Colloid Polym Sci 277:846–855
2. Ganachaud F, Sauzedde F, Elaïssari A, Pichot C (1997) J Appl Polym Sci 65:2315
3. Sauzedde F, Ganachaud F, Elaïssari A, Pichot C (1997) J Appl Polym Sci 65:2331
4. Duracher D, Sauzedde F, Elaïssari A, Perrin A, Pichot C (1998) Colloid Polym Sci, 276:219
5. Duracher D, Sauzedde F, Elaïssari A, Pichot C, Nabzar L (1998) Colloid Polym Sci, 276:920
6. Munier F, Elaïssari A, Pichot C (1995) Polym Adv Technol 6:489
7. Kondo A, Kamura H, Higashitani K (1994) Appl Microbiol Biotechnol 41:99
8. Sauzedde F (1997) Thesis. Claude Bernard University, Lyon-1, France
9. Fujimoto K, Mizuhara Y, Tamura N, Kawaguchi H (1993) J Intelligent Mater Syst Struct 4:184
10. Hergeth W-D, Starre P, Schmutzler K, Wartewig S (1988) Polymer 29:1323
11. Furusawa K, Nagashima K, Anzai C (1994) Colloid Polym Sci 272:1104
12. Yanase N, Noguchi H, Asakura H, Suzuta T (1993) J Appl Polym Sci 50:765
13. Haga Y, Watanabe T, Yosomiya R (1991) Angew Makromol Chem 189:23
14. Hofman-Caris CHM (1994) New J Chem 18:1087
15. Li X, Sun Z (1995) J Appl Polym Sci 58:1991
16. Bourgeat-Lami E, Espiard P, Guyot A (1995) Polymer 36:4385
17. Caris CHM, van Elven LPM, van Herk A, German AL (1989) Br Polym J 21:133